THE JOURNAL OF PHYSICAL CHEMISTRY C

Article

pubs.acs.org/JPCC

A Non-Thermal Plasma Route to Plasmonic TiN Nanoparticles

Alejandro Alvarez Barragan,[†] Niranjan V. Ilawe,[‡] Lanlan Zhong,[§] Bryan M. Wong,[‡,§] and Lorenzo Mangolini*[,†,§]

[†]Department of Mechanical Engineering, University of California—Riverside, Riverside, California 92521, United States

[‡]Department of Chemical and Environmental Engineering, University of California—Riverside, Riverside, California 92521, United States

[§]Materials Science and Engineering Program, University of California—Riverside, Riverside, California 92521, United States

Supporting Information

ABSTRACT: In this contribution, we present a high-throughput method for the synthesis of titanium nitride nanoparticles. The technique, based on a continuous-flow nonthermal plasma process, leads to the formation of free-standing titanium nitride particles with crystalline structures and below 10 nm in size. Extinction measurements of the as-synthesized particles show a clear plasmonic resonance in the near-infrared region, with a peak plasmon position varying between 800 and 1000 nm. We have found that the composition can be controllably tuned by modifying the process parameters and that the particle optical properties are strongly dependent upon composition. XPS and STEM/EDS analyses suggest that nitrogen-poor particles are more susceptible to oxidation, and the extinction spectra show a decrease and a red-shift in plasmon peak position as the degree of oxidation increases. The role of oxidation is confirmed by real-time, time-dependent density functional tight binding (RT-TDDFTB) calculations, which also predict a decrease in the localized surface plasmon resonance energy when a single monolayer of oxygen is added to the surface of a titanium nitride nanocrystal. This study highlights the opportunity and challenges presented by this material system. Understanding the processing-properties relationships for alternative plasmonic materials such as titanium nitride is essential for their successful use in biomedical, photocatalytic, and optoelectronic applications.

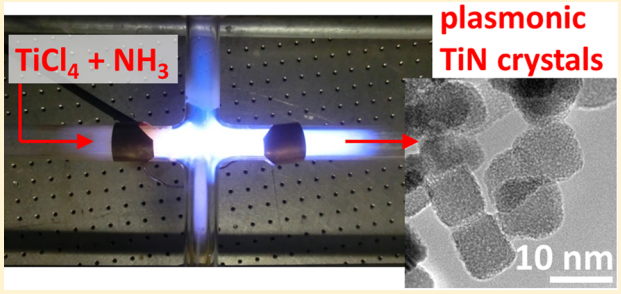

INTRODUCTION

The development of novel plasmonic structures and materials is essential for fields such as biophotonics,[1] photovoltaics,[2] photocatalysis,[3] sensing,[4] and waveguiding.[5] Gold is well-known for having a localized surface plasmon resonance (LSPR) in the visible.[6−8] Its biocompatibility and high chemical stability make it a great candidate for several applications, but its high cost and poor thermal stability, a problem exacerbated by the reduction in melting point observed in nanostructures,[9] limit its utilization. In addition, the design and realization of more complex structures such as gold nanoshells is needed to red-shift the LSPR peak toward the so-called biological transparency window, a region in the near-infrared regime where light is mostly transmitted through biological tissue.[10,11] These considerations motivate recent efforts on the development of alternative plasmonic materials that can overcome the limitation of precious-metal-based plasmonics. The objectives of the work summarized in this manuscript are to (a) describe a novel approach for the synthesis of high-quality titanium nitride nanocrystals with plasmonic response and (b) discuss the influence of oxidation on the properties of small titanium nitride nanoparticles. We focus on titanium nitride (TiN) because of its high melting point and good chemical stability.[12] TiN shows an active LSPR in the NIR region,[13,14] and TiN nanoparticles outperform gold in local heating enhancement in the biological transparency window.[15] A well-documented growth of a native oxide layer on TiN films motivates the use of TiN-TiO_2 nanostructures for photocatalytic applications in high-temperature environments.[16] Moreover, TiN may offer an additional degree of freedom in the tuning of its optical properties compared to silver and gold-based plasmonics, whose response is typically controlled by engineering nanoparticle size and shape.[17,18] Careful characterization of the optical properties of sputtered TiN films reveals that changes in the titanium-to-nitrogen ratio affect both the plasma frequency and relaxation time of conduction electrons,[19] opening the possibility of controlling the position of the plasmonic response by compositional tuning.

Considering that the position of the plasmon peak is highly dependent on particle size and composition, an adequate control of these parameters is crucially important to advance the field. Scalability of the process is equally important to break into mass-production markets. TiN nanoparticles have been prepared by nitridation of precursor powders,[20] laser ablation in

Received: September 3, 2016
Revised: December 29, 2016
Published: January 3, 2017

DOI: 10.1021/acs.jpcc.6b08910
J. Phys. Chem. C 2017, 121, 2316−2322

solution,[21] microwave and thermal plasma,[22,23] and other chemical routes.[24] These methods have limitations such as the need for high-temperature environments and low processing rate (nitridation of precursor powders at 800 °C for 5 h), use of specialized laser equipment and production of nonfree-standing particles (laser ablation in solution), and broad particle-size distribution (microwave and thermal plasmas). The nonthermal plasma synthesis of nanoparticles can overcome these limitations. This approach is characterized by high chemical reactivity,[25] by the unipolar charging of particles suspended in the plasma,[26] and by a high rate of nanoparticle heating induced by the interaction between the particles and the plasma-produced radicals.[25,27,28] These translate into the capability of producing powders composed of a wide range of materials (Si,[29] Si−Ge,[30] ZnO,[31] and SiC[32]), with a small size and narrow size distribution, and with a high-quality crystalline structure. In this manuscript, we report for the first time the utilization of a similar procedure for the production of TiN nanoparticles, highlighting the possibility to tune their optical properties by modifying controllable process parameters such as ammonia flow rate. An in-depth study of the nanoparticles structure, as well as the effects of oxidation in their optical properties is also presented. To complement our experimental results, we investigated the effect that a surface oxide layer has on the optical properties of TiN nanoparticles by using large-scale, real-time quantum dynamics calculations.

EXPERIMENTAL AND THEORETICAL METHODS

Experimental. The synthesis of TiN nanoparticles is based on the continuous-flow nonthermal plasma reactor design described by Mangolini et al.,[29] and consists in supplying the appropriate titanium and nitrogen precursors to a plasma sustained by a 13.56 MHz (RF) power supply. A simplified schematic of this system is shown in Figure S1. Titanium tetrachloride ($TiCl_4$) and ammonia (NH_3) are used as precursors. The reactor is composed of a 25.4 mm outer diameter quartz tube with a thin copper plate wrapped around it as a powered electrode. The width of the copper plate is also 25.4 mm. The vacuum flange upstream of the powered electrode serves as an electrical ground. The distance between the flange and the powered electrode is 50 mm. The RF power supplied to the reactor is 180 W. This power is the minimum necessary to consistently produce crystalline nanoparticles. $TiCl_4$ is delivered using a bubbler kept at atmospheric pressure and in a water bath at 22 °C. Argon (70 sccm) is used as a carrier gas. On the basis of the vapor pressure of $TiCl_4$,[30,33] we estimate the $TiCl_4$ flow rate to be 1 sccm. The pressure in the reactor is set at 3 Torr. TiN nanoparticles are collected downstream from the reactor on a stainless steel mesh filter. After collection, we have found that it is necessary to heat up the sample in a tube furnace at 200 °C under argon atmosphere in order to evaporate ammonium salts, which are a byproduct of the $TiCl_4$−NH_3 reaction.[34] XRD characterization is performed on a PANalytical Empyrean X-ray system using Cu Kα radiation with a wavelength of 1.54 Å. TEM and STEM imaging are performed with a FEI Titan Themis 300 instrument with energy dispersive X-ray Spectroscopy (EDS) capability. EDS spectra were processed using a Bruker Instruments Esprit 1.9 software. Quantification is based on the Cliff-Lorimer approach using calculated k-factors and correcting for thickness by estimating the size of the aggregated particles. Extinction measurements are performed on a Varian Carry 500 UV−vis-NIR spectrophotometer. Samples were prepared by diluting 1 mg of powder in 5 mL of 99.9% methanol to form a clear solution. X-ray photoelectron spectroscopy (XPS) characterization is carried out by using a Kratos AXIS ULTRA^{DLD} XPS system equipped with an Al Kα monochromated X-ray source and a 165 mm mean radius electron energy hemispherical analyzer. Vacuum pressure was kept below 3×10^{-9} Torr during acquisition. A 3 kV Ar-ion beam was used to sputter the particles' surface.

Theoretical. We carried out our electronic calculations using the self-consistent density functional tight-binding (SCC-DFTB) formalism. For probing the optical properties (such as the absorbance spectrum) of our nanoparticles, we implemented and utilized a locally modified real-time, time-dependent DFTB (RT-TDDFTB) code, which is based on the real-time quantum mechanical propagation of the one electron density matrix. This formalism has been previously used to probe the nonequilibrium electron dynamics in several large chemical systems,[35] including photoinjection dynamics in dye-sensitized TiO_2 solar cells[36,37] and many-body interactions in solvated nanodroplets.[38] On the basis of our XRD structure analyses, we optimized the rock-salt arrangement of bulk TiN using the DFTB+ code.[39] Next, a 2.8 nm diameter spherical cluster was cut out of this bulk TiN and used for the subsequent absorbance spectrum calculations. We chose a 2.8 nm diameter cluster (which contains 1189 atoms) because this is near the limit of our computational resources for the time-dependent DFTB calculations (see Supporting Information for computational details). Similarly, for generating the TiO_2-coated TiN cluster, we optimized the anatase structure of bulk TiO_2, which is known to be the more stable phase, particularly in nanocrystalline clusters of TiO_2.[40,41] A spherical shell structure, cut out of the optimized TiO_2 bulk, and a spherical core cut out of the previously optimized TiN bulk were conjoined to form a core−shell structure. The TiO_2 shell thickness was set to 2 Å, and the TiN core diameter was set to 2.4 nm. A full description of our theoretical approach is described in the Supporting Information.

RESULTS AND DISCUSSION

Structural Characterization. For the current design, based on a 25.4 mm diameter reactor, we measure a production rate of free-standing powder of ∼50 mg/h, corresponding to a titanium precursor utilization of 30%. Particle size and composition are highly dependent on the amount of NH_3 introduced into the system. Figure 1a shows XRD data for samples synthesized under different NH_3 flow rate conditions. Reflections of cubic TiN are clearly identified in every sample with peaks at 36.6°, 42.6°, 61.8°, 74.1°, and 77.9° corresponding to the (1 1 1), (2 0 0), (2 2 0), (3 1 1), and (2 2 2) planes of rock-salt TiN. Scherrer analysis indicates an increase in crystallite size from ∼4 nm to ∼8 nm when running the system with 6 and 1.5 sccm of NH_3, respectively. In good agreement with the XRD findings, particle-size distributions (Figure 1b,c) obtained by analyzing TEM micrographs confirm that particles produced with less NH_3 are bigger than those produced at higher NH_3 flow rates (Figure S2). This dependence of particle size as a function of the titanium-to-nitrogen precursor ratio becomes evident for NH_3 flow rates under 10 sccm (i.e., for a $TiCl_4/NH_3$ ratio higher than ∼0.2; see Figure 1d). The biggest particles—produced at 1.5 sccm of NH_3—have a characteristic cubic morphology that has been reported elsewhere (Figure 1e).[16] Moreover, the selected area diffraction pattern shown in the inset is also consistent with the

DOI: 10.1021/acs.jpcc.6b08910
J. Phys. Chem. C 2017, 121, 2316−2322

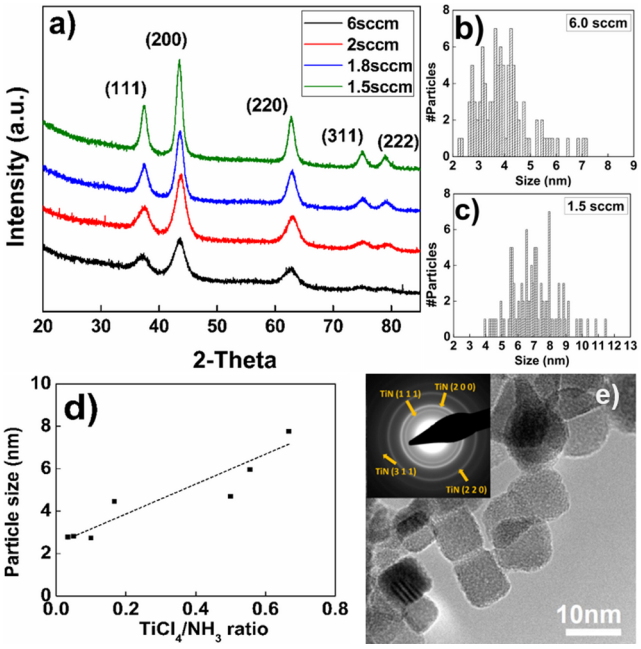

Figure 1. (a) X-ray diffraction of TiN nanoparticles synthesized under different NH_3 flow rate conditions. (b), (c) Particle-size distribution of samples produced at (b) 6 sccm and (c) 1.5 sccm of NH_3. (d) Dependence of particle size determined by Scherrer's formula on the ratio between titanium and nitrogen precursors. (e) TEM micrograph of particles synthesized with 1.5 sccm of NH_3.

XRD reflections from Figure 1a. Additional high-magnification TEM micrographs can be found in Figure S3.

Oxidation Stability and Optical Properties. The LSPR peak of plasmonic metallic nanoparticles is mainly dependent on their shape, size, and surrounding medium.[17,42] However, composition-based control of optical properties is impossible with pure-metal nanoparticles. The nature of the TiN system enables the use of this additional degree of freedom. The extinction spectra of TiN nanoparticles produced with different ammonia flow rates and dispersed in methanol are shown in Figure 2. The spectra are normalized at 350 nm. There is evidence of LSPR peaks in every curve. The peak position varies with processing parameters, ranging from 1000 nm for the particles produced with the higher ammonia flow rate ($NH_3/TiCl_4$ = 6) to 800 nm for those produced with the smaller ammonia flow rate ($NH_3/TiCl_4$ = 1.5). The plasmon peak is narrower and more intense when its position is at a lower wavelength. Differences are obvious even by visual inspection (Figure S4), with particles having a peak LSPR position at 1000 nm appearing yellow and particles with a peak at 800 nm appearing blue under white light illumination.

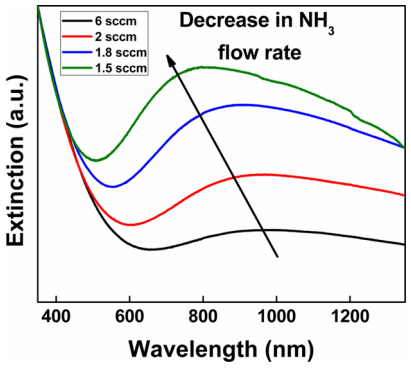

Figure 2. Extinction spectra of TiN nanoparticles produced with different ammonia-to-titanium tetrachloride ratios.

The analysis summarized in Figure 1 suggests that an increase in $NH_3/TiCl_4$ ratio leads to a smaller nanoparticle size, yet these particles have a red-shifted LSPR peak compared to larger particles produced with a smaller $NH_3/TiCl_4$ ratio. This trend is opposite to what the Mie theory predicts,[43,44] suggesting that there are additional factors affecting the optical response of the material. To address this issue, we have carefully investigated the degree of nanoparticle oxidation for materials produced with different processing parameters. The Ti 2p XPS spectra shown in Figure 3 provide important insight on how oxygen is distributed in different-sized particles. The TiO_2 signal (~458.2 and ~463.7 eV)[45] is evident in both small and big particles (Figure 3a,b, respectively). However, shoulders at ~455.0 and ~461.3 eV clearly indicate the presence of TiN,[45] especially in the bigger particles. The substantial amount of oxygen detected may imply these are actually oxynitride nanoparticles. The formation of rock salt titanium oxynitride (TiON) microspheres with an absorbance band in the near-infrared has been reported in the literature.[46] To discard this possibility, we performed additional XPS measurements after a sputtering process to gain some information on the oxygen distribution in the particle core. For the case of the smaller particles, the characteristic TiO_2 peaks are still present after a 150 s sputtering treatment (Figure 3c). However, the oxide-related signals are clearly much weaker than the nitride peaks for the bigger particles (Figure 3d). We estimate a sputter depth of ~1.5 nm and ~3 nm after 10 and 150 s of treatment, respectively, based on the formula reported by McCafferty et al. on their study on XPS sputter profiling of air-oxidized titanium films.[47] From this data, it is evident that oxidation is relevant in TiN nanoparticles but that the extent of the oxidation is higher for particles produced at a higher ammonia flow rate (smaller particles). Moreover, we have confirmed that for the case of the bigger particles most of the oxidation occurs at the surface, while the bulk is mainly composed of TiN. Table 1 summarizes the results of complementary STEM/EDS measurements for particles produced at high ammonia flow rate (small particles) and at low ammonia flow rate (big particles). The data summarized in Table 1 are obtained by sampling the signal over a large number of particles (we estimate a few hundreds in the field of view). The EDS data show low oxygen levels and a very-close-to-stoichiometry N-to-Ti ratio for the bigger particles. On the other hand, smaller particles show higher oxygen levels and a considerably lower N-to-Ti ratio. Overall, and in good agreement with XPS characterization, small particles appear to be nitrogen deficient and oxygen rich, whereas bigger particles are very close to stoichiometry and have a significantly lower oxygen level.

Overall the combination of the XPS and the STEM/EDS data confirm that the bigger particles, produced with a lower $NH_3/TiCl_4$ ratio, are stoichiometric and have an oxide-rich surface. Smaller particles are nitrogen-poor and show a clear sign of oxidation not only at the surface but at the core of the particle as well. The nonthermal plasma process utilized for the synthesis of these particles is effectively oxygen free because the reactor has a negligible leakage rate (2.06×10^{-5} Pa·m^3·s^{-1}), and all the precursors are of ultrahigh purity grade. Oxidation occurs when the particles are extracted from the system and

DOI: 10.1021/acs.jpcc.6b08910
J. Phys. Chem. C 2017, 121, 2316−2322

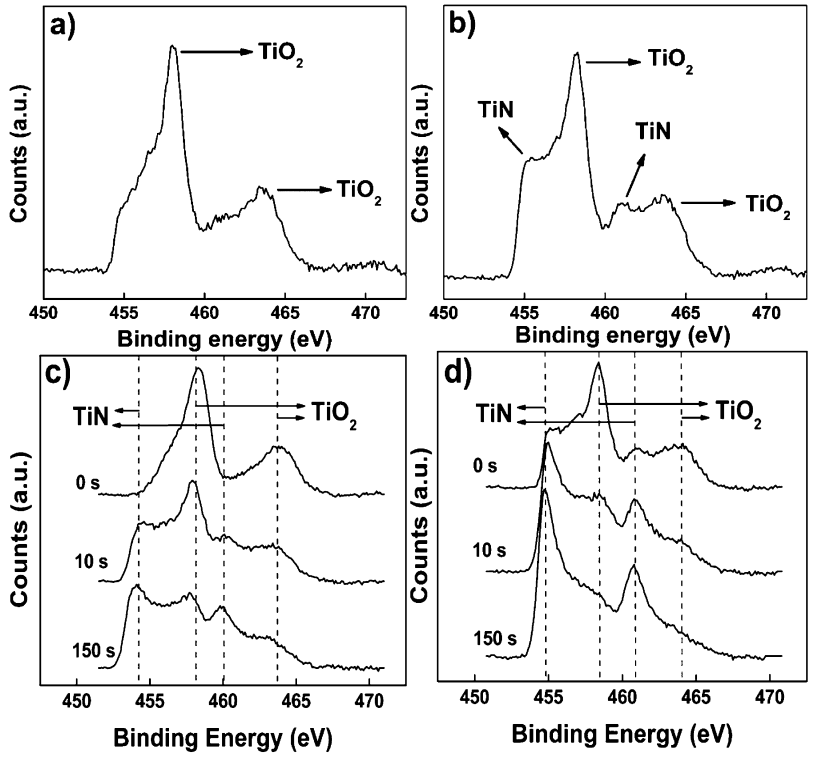

Figure 3. XPS spectra at the surface of (a) small particles produced with a $NH_3/TiCl_4$ ratio of 6 and (b) bigger particles produced with a $NH_3/TiCl_4$ ratio of 1.5. XPS spectra after two sputtering steps on (c) small particles produced with a $NH_3/TiCl_4$ ratio of 6 and (d) bigger particles produced with a $NH_3/TiCl_4$ ratio of 1.5.

Table 1. Composition of Samples Produced with High NH_3 Flow Rate (Small Particles) and Low NH_3 Flow Rate (Big Particles)

element	high NH_3 flow small particles	low NH_3 flow big particles
Ti at%	46.22 ± 4.4	42.1 ± 2.5
N at%	27.6 ± 7.5	42 ± 3.9
O at%	26.18 ± 5.3	15.9 ± 3.3
N/Ti	0.60	0.99

exposed to air. It is reasonable to expect that the high density of vacancies in the nitrogen-deficient particles makes them more susceptible to oxidation, with oxygen clearly diffusing within the core of the particles. This vacancy-induced oxidation mechanism has been reported for other refractory materials such as ZrC.[48]

Role of Oxidation on the Plasmonic Response. We have investigated the role of oxidation on the plasmonic response of TiN particles by monitoring the changes in their optical properties after annealing in air. Figure 4 shows the results of an oxidation experiment where a sample of large particles was air-annealed first at 150 °C and then at 250 °C for 1 h at each temperature. These particles were produced with a low ammonia flow rate, under conditions that lead to a stoichiometric TiN particle core (see Figure 3b,d, and third column in Table 1). The plasmonic response of the particles after annealing in air is remarkably similar to that observed in Figure 2 for nitrogen-poor, oxygen-rich particles. This experiment provides conclusive evidence that the degree of oxidation clearly affects the LSPR peak position and width. The blue-shift in LSPR peak position detected for bigger particles (Figure 2) is not a consequence of size but of composition. Nitrogen-deficient particles are more prone to oxidation due to the high

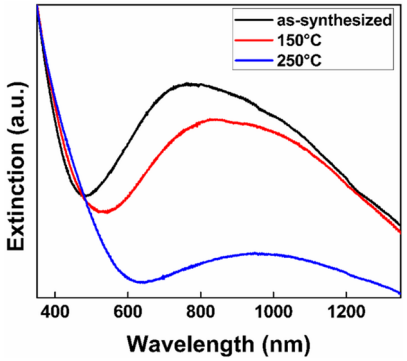

Figure 4. Extinction measurements on ~8 nm TiN nanoparticles before and after air-annealing at 150 and 250 °C.

degree of vacancy defects present in their structure. Finally, we verify the plasmonic nature of the near-infrared peak observed in the extinction spectra in Figure 5. We diluted the same batch of particles in two different solvents (methanol and toluene, n = 1.32 and n = 1.49, respectively). The toluene solution red-shifted relative to that of methanol. This effect is in good agreement with an in-depth study on solvent-dependence of the LSPR position on silver nanoparticles.[49]

RT-TDDFTB Calculations. To complement and support our experimental results, we calculated the optical properties of TiN nanoparticles to understand how the plasmon peak absorbance band is modified by the surface layer properties. Figure 6c plots the RT-TDDFTB absorbance spectrum of a 2.8 nm diameter TiN nanoparticle without a TiO_2 shell (Figure 6a) and a 2.4 nm diameter TiN nanoparticle with a 2 Å thick TiO_2 layer (Figure 6b). A strong peak, corresponding to the plasmon energy, is observed at around 2 eV (615 nm) for the pure TiN

DOI: 10.1021/acs.jpcc.6b08910
J. Phys. Chem. C 2017, 121, 2316−2322

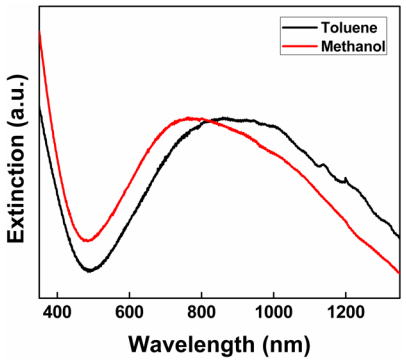

Figure 5. Extinction measurements on ∼8 nm TiN nanoparticles in solvents with different refractive indexes ($n_{methanol}$ = 1.33, $n_{toluene}$ = 1.49).

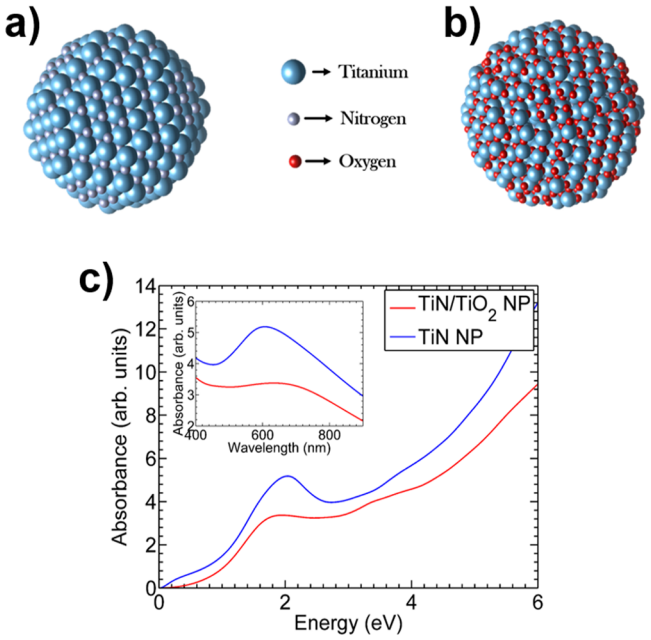

Figure 6. Absorbance spectra of the pure TiN (blue line) and the TiO_2-coated TiN (red line) nanoparticles. The same spectra are shown in the inset with wavelength on the *x*-axis.

particle. Previous computational studies on various titanium nitride nanostructures have reported plasmon energy values that match closely with these RT-TDDFTB results.[15,50] The absorbance spectrum of the TiN/TiO_2 nanoparticle shows a clear reduction in the energy of the LSPR peak relative to that of the pure TiN nanoparticle. This observation directly supports our experimental results and strongly implies that the surface oxide layer (1) plays an important part in controlling the optical properties of the TiN nanoparticles and (2) even a thin oxide surface layer (2 Å) can significantly alter the optical properties of these nanoparticles. These calculations support our experimental findings that the LSPR peak position is strongly dependent on the degree of oxidation.

It is apparent that the nonthermal plasma process tends to produce nitrogen-poor and smaller particles when the NH_3 flow rate is increased with respect to the $TiCl_4$ flow rate. While this is counterintuitive, the exact mechanism leading to the nucleation and growth of TiN particles in this kind of reactive system is completely unexplored at this point and will be the subject of future contributions. Nevertheless, based on our previous experience with the synthesis of nanoparticles using nonthermal plasma reactors,[28,51] we expect an increase in the vapor pressure of molecular species such as NH_3 to lead to a quenching of the discharge, in turn leading to a decrease in the density of chemically reactive species (radicals such as atomic nitrogen) likely responsible for the nitridation of the particles.

CONCLUSIONS

We have successfully applied a continuous-flow nonthermal plasma synthesis technique to the case of TiN nanoparticles. Plasma-produced TiN particles show a plasmonic peak in the near-infrared part of the spectrum, and the position of the LSPR peak can be controlled by tuning process parameters such as the $NH_3/TiCl_4$ ratio. A combination of XPS and STEM/EDS analysis suggest that the red-shift in the LSPR peak is observed in particles with a lower N/Ti ratio (i.e., nitrogen-poor particles). Due to the high concentration of vacancies, these particles are particularly prone to oxidation after production, upon exposure to air. Particles produced at stoichiometric conditions still show an oxide-rich surface layer and are susceptible to oxidation after annealing in air at temperatures as low as 150 °C. The annealing in air is accompanied by a red-shift in plasmon peak position, consistent with the explanation that the oxide layer reduces the energy of the plasmon resonance. Experimental results are in good agreement with large-scale real-time, time-dependent DFTB simulations performed on pure TiN and TiO_2-coated TiN nanoparticles. This contribution, while describing a novel approach to the production of novel plasmonic nanoparticles with narrow size distribution and controllable composition, highlights the need for more extensive studies on this complex material when in nanoparticle form, especially with respect to oxidation kinetics and its influence on optoelectronic properties.

ASSOCIATED CONTENT

Supporting Information

The Supporting Information is available free of charge on the ACS Publications website at DOI: 10.1021/acs.jpcc.6b08910.

Computational details, experimental setup, TEM micrographs of small and big particles, additional high-resolution TEM micrographs with selected area diffraction patterns, colloidal solutions of small and big particles under white light illumination, STEM/EDS mapping of big and small particles (PDF)

AUTHOR INFORMATION

Corresponding Author

*E-mail: lmangolini@engr.ucr.edu.

ORCID

Bryan M. Wong: 0000-0002-3477-8043

Lorenzo Mangolini: 0000-0002-0057-2450

Notes

The authors declare no competing financial interest.

ACKNOWLEDGMENTS

This work was primarily supported by the U.S. Department of Energy, Office of Science, Early Career Research Program under Award No. DE-SC0014169. We acknowledge the National Science Foundation under grant DMR-0958796 for support with the XPS characterization. A.A.B. acknowledges the

DOI: 10.1021/acs.jpcc.6b08910
J. Phys. Chem. C 2017, 121, 2316−2322

support of the "Consejo Nacional de Ciencia y Tecnología" (CONACYT, Mexico) and The University of California Institute for Mexico and the United States (UC MEXUS). RT-TDDFTB calculations by N.V.I. and B.M.W. were supported by the U.S. Department of Energy, Office of Science, Early Career Research Program under Award No. DE-SC0016269. STEM/EDS characterization was performed at the Central Facility for Advanced Microscopy and Microanalysis (CFAMM) at UC Riverside.

REFERENCES

(1) Hirsch, L. R.; Stafford, R. J.; Bankson, J. A.; Sershen, S. R.; Rivera, B.; Price, R. E.; Hazle, J. D.; Halas, N. J.; West, J. L. Nanoshell-Mediated near-Infrared Thermal Therapy of Tumors Under Magnetic Resonance Guidance. *Proc. Natl. Acad. Sci. U. S. A.* **2003**, *100*, 13549−13554.

(2) Clavero, C. Plasmon-Induced Hot-Electron Generation at Nanoparticle/metal-Oxide Interfaces for Photovoltaic and Photocatalytic Devices. *Nat. Photonics* **2014**, *8*, 95−103.

(3) Kale, M. J.; Avanesian, T.; Christopher, P. Direct Photocatalysis by Plasmonic Nanostructures. *ACS Catal.* **2014**, *4*, 116−128.

(4) Liao, H.; Nehl, C. L.; Hafner, J. H. Biomedical Applications of Plasmon Resonant Metal Nanoparticles. *Nanomedicine* **2006**, *1*, 201−208.

(5) Lal, S.; Link, S.; Halas, N. J. Nano-Optics from Sensing to Waveguiding. *Nat. Photonics* **2007**, *1*, 641−648.

(6) Daniel, M.-C.; Astruc, D. Gold Nanoparticles: Assembly, Supramolecular Chemistry, Quantum-Size-Related Properties, and Applications Toward Biology, Catalysis, and Nanotechnology. *Chem. Rev.* **2004**, *104*, 293−346.

(7) Chan, G. H.; Zhao, J.; Hicks, E. M.; Schatz, G. C.; Van Duyne, R. P. Plasmonic Properties of Copper Nanoparticles Fabricated by Nanosphere Lithography. *Nano Lett.* **2007**, *7*, 1947−1952.

(8) Mock, J. J.; Barbic, M.; Smith, D. R.; Schultz, D. A.; Schultz, S. Shape Effects in Plasmon Resonance of Individual Colloidal Silver Nanoparticles. *J. Chem. Phys.* **2002**, *116*, 6755−6759.

(9) Goldstein, A. N.; Echer, C. M.; Alivisatos, A. P. Melting in Seminconductor Nanocrystals. *Science* **1992**, *256*, 1425−1427.

(10) Oldenburg, S. J.; Jackson, J. B.; Westcott, S. L.; Halas, N. J. Infrared Extinction Properties of Gold Nanoshells. *Appl. Phys. Lett.* **1999**, *75*, 2897−2899.

(11) Tsai, M.-F.; Chang, S.-H. G.; Cheng, F.-Y.; Shanmugam, V.; Cheng, Y.-S.; Su, C.-H.; Yeh, C.-S. Au Nanorod Design as Light-Absorber in the First and Second Biological near-Infrared Windows for in Vivo Photothermal Therapy. *ACS Nano* **2013**, *7*, 5330−5342.

(12) Patsalas, P.; Logothetidis, S. Optical, Electronic, and Transport Properties of Nanocrystalline Titanium Nitride Thin Films. *J. Appl. Phys.* **2001**, *90*, 4725−4734.

(13) Quinten, M. The Color of Finely Dispersed Nanoparticles. *Appl. Phys. B: Lasers Opt.* **2001**, *73*, 317−326.

(14) Reinholdt, A.; Pecenka, R.; Pinchuk, A.; Runte, S.; Stepanov, A. L.; Weirich, T. E.; Kreibig, U. Structural, Compositional, Optical and Colorimetric Characterization of TiN-Nanoparticles. *Eur. Phys. J. D* **2004**, *31*, 69−76.

(15) Guler, U.; Naik, G. V.; Boltasseva, A.; Shalaev, V. M.; Kildishev, A. V. Performance Analysis of Nitride Alternative Plasmonic Materials for Localized Surface Plasmon Applications. *Appl. Phys. B: Lasers Opt.* **2012**, *107*, 285−291.

(16) Guler, U.; Suslov, S.; Kildishev, A. V.; Boltasseva, A.; Shalaev, V. M. Colloidal Plasmonic Titanium Nitride Nanoparticles: Properties and Applications. *Nanophotonics* **2015**, *4*, 269−276.

(17) Link, S.; El-Sayed, M. A. Shape and Size Dependence of Radiative, Non-Radiative and Photothermal Properties of Gold Nanocrystals. *Int. Rev. Phys. Chem.* **2000**, *19*, 409−453.

(18) Amendola, V.; Bakr, O. M.; Stellacci, F. A Study of the Surface Plasmon Resonance of Silver Nanoparticles by the Discrete Dipole Approximation Method: Effect of Shape, Size, Structure, and Assembly. *Plasmonics* **2010**, *5*, 85−97.

(19) Kang, J. H.; Kim, K. J. Structural, Optical, and Electronic Properties of Cubic TiNx Compounds. *J. Appl. Phys.* **1999**, *86*, 346−350.

(20) Li, J.; Gao, L.; Sun, J.; Zhang, Q.; Guo, J.; Yan, D. Synthesis of Nanocrystalline Titanium Nitride Powders by Direct Nitridation of Titanium Oxide. *J. Am. Ceram. Soc.* **2001**, *84*, 3045−3047.

(21) Takada, N.; Sasaki, T.; Sasaki, K. Synthesis of Crystalline TiN and Si Particles by Laser Ablation in Liquid Nitrogen. *Appl. Phys. A: Mater. Sci. Process.* **2008**, *93*, 833−836.

(22) Tavares, J.; Coulombe, S.; Meunier, J. L. Synthesis of Cubic-Structured Monocrystalline Titanium Nitride Nanoparticles by Means of a Dual Plasma Process. *J. Phys. D: Appl. Phys.* **2009**, *42*, 102001.

(23) Kumar, S. M.; Murugan, K.; Chandrasekhar, S. B.; Hebalkar, N.; Krishna, M.; Satyanarayana, B. S.; Madras, G. Synthesis and Characterization of Nano Silicon and Titanium Nitride Powders Using Atmospheric Microwave Plasma Technique. *J. Chem. Sci.* **2012**, *124*, 557−563.

(24) Zhang, H.; Li, F.; Jia, Q. Preparation of Titanium Nitride Ultrafine Powders by Sol−gel and Microwave Carbothermal Reduction Nitridation Methods. *Ceram. Int.* **2009**, *35*, 1071−1075.

(25) Lopez, T.; Mangolini, L. On the Nucleation and Crystallization of Nanoparticles in Continuous-Flow Nonthermal Plasma Reactors. *J. Vac. Sci. Technol., B: Nanotechnol. Microelectron.: Mater., Process., Meas., Phenom.* **2014**, *32*, 061802.

(26) Kortshagen, U.; Bhandarkar, U. Modeling of Particulate Coagulation in Low Pressure Plasmas. *Phys. Rev. E: Stat. Phys., Plasmas, Fluids, Relat. Interdiscip. Top.* **1999**, *60*, 887−898.

(27) Mangolini, L.; Kortshagen, U. Selective Nanoparticle Heating: Another Form of Nonequilibrium in Dusty Plasmas. *Phys. Rev.* **2009**, *79*, 026405.

(28) Lopez, T.; Mangolini, L. In Situ Monitoring of Hydrogen Desorption from Silicon Nanoparticles Dispersed in a Nonthermal Plasma. *J. Vac. Sci. Technol., B: Nanotechnol. Microelectron.: Mater., Process., Meas., Phenom.* **2016**, *34*, 041206.

(29) Mangolini, L.; Thimsen, E.; Kortshagen, U. High-Yield Plasma Synthesis of Luminescent Silicon Nanocrystals. *Nano Lett.* **2005**, *5*, 655−659.

(30) Yasar-Inceoglu, O.; Mangolini, L. Characterization of Si−Ge Alloy Nanocrystals Produced in a Non-Thermal Plasma Reactor. *Mater. Lett.* **2013**, *101*, 76−79.

(31) Greenberg, B. L.; Ganguly, S.; Held, J. T.; Kramer, N. J.; Mkhoyan, K. A.; Aydil, E. S.; Kortshagen, U. R. Nonequilibrium-Plasma-Synthesized ZnO Nanocrystals with Plasmon Resonance Tunable via Al Doping and Quantum Confinement. *Nano Lett.* **2015**, *15*, 8162−8169.

(32) Coleman, D.; Lopez, T.; Yasar-Inceoglu, O.; Mangolini, L. Hollow Silicon Carbide Nanoparticles from a Non-Thermal Plasma Process. *J. Appl. Phys.* **2015**, *117*, 193301.

(33) Pearce, M. L.; McCabe, N. R. The Vapour Pressure of Titanium Tetrachloride. *J. Inorg. Nucl. Chem.* **1965**, *27*, 1876−1878.

(34) Elers, K.-E.; Saanila, V.; Soininen, P. J.; Li, W.-M.; Kostamo, J. T.; Haukka, S.; Juhanoja, J.; Besling, W. F. Diffusion Barrier Deposition on a Copper Surface by Atomic Layer Deposition. *Chem. Vap. Deposition* **2002**, *8*, 149−153.

(35) Oviedo, M. B.; Negre, C. F. A.; Sánchez, C. G. Dynamical Simulation of the Optical Response of Photosynthetic Pigments. *Phys. Chem. Chem. Phys.* **2010**, *12*, 6706−6711.

(36) Negre, C. F. A.; Fuertes, V. C.; Oviedo, M. B.; Oliva, F. Y.; Sánchez, C. G. Quantum Dynamics of Light-Induced Charge Injection in a Model Dye−Nanoparticle Complex. *J. Phys. Chem. C* **2012**, *116*, 14748−14753.

(37) Oviedo, M. B.; Zarate, X.; Negre, C. F. A.; Schott, E.; Arratia-Pérez, R.; Sánchez, C. G. Quantum Dynamical Simulations as a Tool for Predicting Photoinjection Mechanisms in Dye-Sensitized TiO_2 Solar Cells. *J. Phys. Chem. Lett.* **2012**, *3*, 2548−2555.

(38) Oviedo, M. B.; Wong, B. M. Real-Time Quantum Dynamics Reveals Complex, Many-Body Interactions in Solvated Nanodroplets. *J. Chem. Theory Comput.* **2016**, *12*, 1862−1871.

DOI: 10.1021/acs.jpcc.6b08910
J. Phys. Chem. C 2017, 121, 2316−2322

(39) Aradi, B.; Hourahine, B.; Frauenheim, T. DFTB+, a Sparse Matrix-Based Implementation of the DFTB Method†. *J. Phys. Chem. A* **2007**, *111*, 5678−5684.
(40) Fuertes, V. C.; Negre, C. F. A.; Oviedo, M. B.; Bonafe, F. P.; Oliva, F. Y.; Sanchez, C. G. A Theoretical Study of the Optical Properties of Nanostructured TiO_2. *J. Phys.: Condens. Matter* **2013**, *25*, 115304.
(41) Naicker, P. K.; Cummings, P. T.; Zhang, H.; Banfield, J. F. Characterization of Titanium Dioxide Nanoparticles Using Molecular Dynamics Simulations. *J. Phys. Chem. B* **2005**, *109*, 15243−15249.
(42) Kreibig, U.; Genzel, L. Optical Absorption of Small Metallic Particles. *Surf. Sci.* **1985**, *156*, 678−700.
(43) Mogensen, K. B.; Kneipp, K. Size-Dependent Shifts of Plasmon Resonance in Silver Nanoparticle Films Using Controlled Dissolution: Monitoring the Onset of Surface Screening Effects. *J. Phys. Chem. C* **2014**, *118*, 28075−28083.
(44) Turkevich, J.; Garton, G.; Stevenson, P. C. The Color of Colloidal Gold. *J. Colloid Sci.* **1954**, *9*, 26−35.
(45) Saha, N. C.; Tompkins, H. G. Titanium Nitride Oxidation Chemistry: An X-Ray Photoelectron Spectroscopy Study. *J. Appl. Phys.* **1992**, *72*, 3072−3079.
(46) Yoo, J. B.; Yoo, H. J.; Jung, H. J.; Kim, H. S.; Bang, S.; Choi, J.; Suh, H.; Lee, J.-H.; Kim, J.-G.; Hur, N. H. Titanium Oxynitride Microspheres with the Rock-Salt Structure for Use as Visible-Light Photocatalysts. *J. Mater. Chem. A* **2016**, *4*, 869−876.
(47) McCafferty, E.; Wightman, J. P. An X-Ray Photoelectron Spectroscopy Sputter Profile Study of the Native Air-Formed Oxide Film on Titanium. *Appl. Surf. Sci.* **1999**, *143*, 92−100.
(48) Hu, W.; Xiang, J.; Liu, S.; Zhang, Y.; Chen, C.; Wang, P.; Wang, H.; Wen, F.; Xu, B.; He, J.; et al. Low-Temperature Diffusion of Oxygen through Ordered Carbon Vacancies in Zr 2 C X: The Formation of Ordered Zr_2 C_xO_y. *Inorg. Chem.* **2012**, *51*, 5164−5172.
(49) Jensen, T. R.; Duval, M. L.; Kelly, K. L.; Lazarides, A. A.; Schatz, G. C.; Van Duyne, R. P. Nanosphere Lithography: Effect of the External Dielectric Medium on the Surface Plasmon Resonance Spectrum of a Periodic Array of Silver Nanoparticles. *J. Phys. Chem. B* **1999**, *103*, 9846−9853.
(50) Cortie, M. B.; Giddings, J.; Dowd, A. Optical Properties and Plasmon Resonances of Titanium Nitride Nanostructures. *Nanotechnology* **2010**, *21*, 115201.
(51) Yasar-Inceoglu, O.; Lopez, T.; Farshihagro, E.; Mangolini, L. Silicon Nanocrystal Production Through Non-Thermal Plasma Synthesis: A Comparative Study Between Silicon Tetrachloride and Silane Precursors. *Nanotechnology* **2012**, *23*, 255604.

DOI: 10.1021/acs.jpcc.6b08910
J. Phys. Chem. C 2017, 121, 2316−2322